Chaotic Pattern Alternations Can Reproduce Properties Of Dominance Durations In Multistable Perception

Takashi Kanamaru

Department of Mechanical Science and Engineering,
School of Advanced Engineering, Kogakuin University,
Hachioji-city, Tokyo 192-0015, Japan

Abstract

We propose a pulse neural network that exhibits chaotic pattern alternations among stored patterns as a model of multistable perception, which is reflected in phenomena such as binocular rivalry and perceptual ambiguity. When we regarded the mixed state of patterns as a part of each pattern, the durations of the retrieved pattern obey unimodal distributions. We confirmed that no chaotic properties are observed in the time series of durations, consistent with the findings of previous psychological studies. Moreover, it is shown that our model also reproduces two properties of multistable perception that characterize the relationship between the contrast of inputs and the durations.

1   Introduction

In the perception of visual information, multistable perception is a well known phenomenon. For example, when two different stimuli are presented to the eyes, the dominant stimulus perceived fluctuates over time, a phenomenon known as binocular rivalry (Levelt, 1967; Walker, 1975; Lehky, 1995; Blake, 2001). Similarly, when an ambiguous figure such as a Necker cube is presented, the dominant interpretation also fluctuates over time (Borsellino et al., 1972; Alais & Blake, 2015). Research has also indicated that the duration of the dominant perception (dominance duration) may be characterized by a unimodal distribution, such as the gamma distribution (Levelt, 1967; Borsellino et al., 1972; Walker, 1975) or the log-normal distribution (Lehky, 1995).

Although many theoretical models have been proposed, the mechanism of such multistable perception is still unknown (Lehky, 1988; Laing & Chow, 2002; Wilson, 2003; Freeman, 2005; Wilson, 2007). Typical models assume that the rivalry takes place between the two eyes, or the two monocular pathways ("eye rivalry") (Lehky, 1988; Wilson, 2007). Such models are composed of two oscillators with reciprocal inhibitions, and the stochastic properties are introduced to the model by adding noise (Lehky, 1988). One possible mechanism for such noise would be associated with fluctuation in the visual system, which is generated by small

eye movements and microsaccades. Laing & Chow (2002) suggested that randomness in their model is caused not by noise but by deterministic chaos inherent in the network.

The eye rivalry is thought to take place between monocular neurons within the primary visual cortex. However, Logothetis et al. (1996) found that neurons whose activity correlates with rivalry were in higher cortical areas. In their experiment, the two stimuli presented to the eyes were swapped every 330 ms. Even under such a condition, the results typical of the binocular rivalry were found, and the mean dominance time of one pattern was 2,350 ms, which is much longer than the swap time of 330 ms. Their results can be interpreted that in higher cortical areas, rivalry takes place between two patterns presented to the eyes (pattern rivalry). Their results show that the pattern rivalry can be modeled using a hierarchical model with two rivalry stages (Wilson, 2003), each of which shows the eye rivalry and the pattern rivalry, respectively. However, a multistage model does not always show the pattern rivalry (Freeman, 2005); therefore, the mechanism of the pattern rivalry is still controversial.

As for such pattern rivalry in the multistable perception, there is related research (Leeuwen et al., 1997; Nagao et al., 2000). Leeuwen et al. (1997) examined a network of the logistic map that yields chaotic dynamics and observed chaotic switching between synchronous state and asynchronous state. Moreover, the distribution of interswitch period between each state was found to be unimodal. Although it is attractive to relate their model to the multistable perception, their model is an abstract one and not based on the knowledge of neuroscience.

Nagao et al. (2000) stored 20 binary patterns in a neuronal network and regarded two patterns as the perceived states. In this network, the retrieved pattern fluctuates chaotically between two patterns. This dynamics is understood in the literature of the chaotic associative memory model in which the state of the network changes chaotically among several patterns (Aihara, Takabe, & Toyoda, 1990; Inoue & Nagayoshi, 1991; Nara & Davis, 1992; Tsuda, 1992; Adachi & Aihara, 1997). Typically the duration of a pattern in the chaotic associative memory model does not obey a unimodal distribution, but it often obeys a monotonically decreasing distribution (Tsuda, 1992). However, the model in Nagao

et al. (2000) successfully reproduces a unimodal distribution of dominance duration.

In the study presented in this letter, we report that the pattern alternations caused by chaotic dynamics of a pulse neural network can also reproduce the properties of multistable perception. This network is composed of neuronal models that emit spikes when a sufficiently strong input is injected, while the previous models of chaotic associative memory were composed of conventional neuronal models based on firing rates. In our network, the durations of the retrieved pattern obey unimodal distributions when we regard the mixed state of patterns as part of each pattern. Moreover, although the pattern alternations are caused by chaotic dynamics, the chaotic properties are not detected in the series of the durations of the retrieved pattern. Therefore, our results are consistent with Lehky (1995), who stated that the statistical properties of binocular rivalry are not chaotic. Moreover, we show that our model can reproduce two characteristics of binocular rivalry. First, when reducing the contrast of a stimulus to one eye, dominance intervals in the other eye increase and dominance intervals in the stimulated eye are relatively unchanged (Laing & Chow, 2002; Wilson, 2007). Second, when increasing the contrast of the stimuli to both eyes, dominance intervals in both eyes decrease (Laing & Chow, 2002; Wilson, 2007).

This letter is organized as follows. In section 2, we define a pulse neural network composed of excitatory neurons and inhibitory neurons exhibiting synchronized, chaotic firing. In the subsequent sections, we refer to this network as the one-module system. In section 3, we connect eight modules of networks in which two patterns are stored according to the mechanism of associative memory. These two patterns correspond to the two stable states of binocular rivalry and perceptual ambiguity. We further show that chaotic dynamics are responsible for alterations in the retrieved patterns over time. In section 4, we show that the durations of the retrieved pattern obey unimodal distributions. In section 5, we examine the dependences of the peak position of the unimodal distribution on the connection strengths and the number of patterns. In section 6, we show that chaotic properties are not detected in the series of the durations of the retrieved pattern. In section 7, we show that our model can reproduce two characteristics of binocular rivalry. Section 8 concludes.

2 One-module system

In sections 2 and 3, we introduce a neural network of theta neurons with phases as their internal states (Ermentrout & Kopell, 1986; Ermentrout, 1996; Izhikevich, 1999, 2000; Kanamaru & Sekine, 2005b). When a sufficiently strong input is provided, each neuron yields a pulse by increasing its phase around a circle and returning to its original phase. The network is composed of N_E excitatory neurons and N_I in-

hibitory neurons governed by the following equations:

$$\dot{\theta}_E^{(i)} = (1 - \cos \theta_E^{(i)}) + (1 + \cos \theta_E^{(i)})$$
$$\times (r_E + \xi_E^{(i)}(t) + g_{int} I_E(t) - g_{ext} I_I(t)) \quad (2.1)$$

$$\dot{\theta}_I^{(i)} = (1 - \cos \theta_I^{(i)}) + (1 + \cos \theta_I^{(i)})$$
$$\times (r_I + \xi_I^{(i)}(t) + g_{ext} I_E(t) - g_{int} I_I(t)) \quad (2.2)$$

$$I_X(t) = \frac{1}{2N_X} \sum_{j=1}^{N_X} \sum_k \frac{1}{\kappa_X} \exp\left(-\frac{t - t_k^{(j)}}{\kappa_X}\right), \quad (2.3)$$

$$\langle \xi_X^{(i)}(t) \xi_Y^{(j)}(t') \rangle = D \delta_{XY} \delta_{ij} \delta(t - t'), \quad (2.4)$$

where $\theta_E^{(i)}$ and $\theta_I^{(i)}$ are the phases of the ith excitatory neuron and the ith inhibitory neuron, respectively. r_E and r_I are parameters of the neurons that determine whether the equilibrium of each neuron is stable. We used $r_E = r_I = -0.025$ to ensure that each neuron had a stable equilibrium. $X = E$ or I denote the excitatory or inhibitory ensemble, respectively, while $t_k^{(j)}$ is the kth firing time of the jth neuron in the ensemble X and the firing time is defined as the time at which $\theta_X^{(j)}$ exceeds π in the positive direction. The neurons communicate with each other using the postsynaptic potentials whose waveforms are the exponential functions, as shown in equation 2.3. $\xi_X^{(i)}(t)$ represents gaussian white noise added to the ith neuron in the ensemble X.

Throughout the remainder of the letter, this network is referred to as a one-module system that exhibits various patterns of synchronized firing (Kanamaru & Sekine, 2005b). We utilized the chaotic synchronization shown in Figure 1. Figure 1A shows a raster plot of spikes of 200 randomly chosen excitatory neurons and inhibitory neurons in a module with $N_E = N_I = 2000$. This plot allows one to observe the synchronized firing of neurons and that the intervals of synchronized firing do not remain constant. The instantaneous firing rates J_E and J_I of the excitatory and inhibitory ensembles calculated from the data used in Figure 1A are shown in Figure 1B. A trajectory of J_E and J_I in the (J_E, J_I) plane is also shown in Figure 1C, revealing somewhat complex structures. To analyze these structures, we took the limit of $N_E, N_I \to \infty$ in order to obtain the Fokker-Planck equation, which governs the dynamics of the probability densities $n_E(\theta_E)$ and $n_I(\theta_I)$ of $\theta_E^{(i)}$ and $\theta_I^{(i)}$, as shown in Appendix A. J_E and J_I, obtained from the analysis of the Fokker-Planck equation, are shown in Figures 1E and 1F. In Figure 1F, a fine structure of a strange attractor is observed. The largest Lyapunov exponent of the attractor in Figure 1F is positive (Kanamaru & Sekine, 2005b), indicating that the dynamics of J_E and J_I are chaotic. Moreover, the asynchronous firings shown in Figure 1D coexist with the chaotic synchronization shown in Figure 1A because each neuron has stable equilibrium. This coexistence of two states is important for realizing chaotic pattern alternations.

In the following sections, only the one-module systems with infinite neurons treated in Figures 1E and 1F are considered, as the Fokker-Planck equation does not contain noise, allowing for the reproduction of analyses.
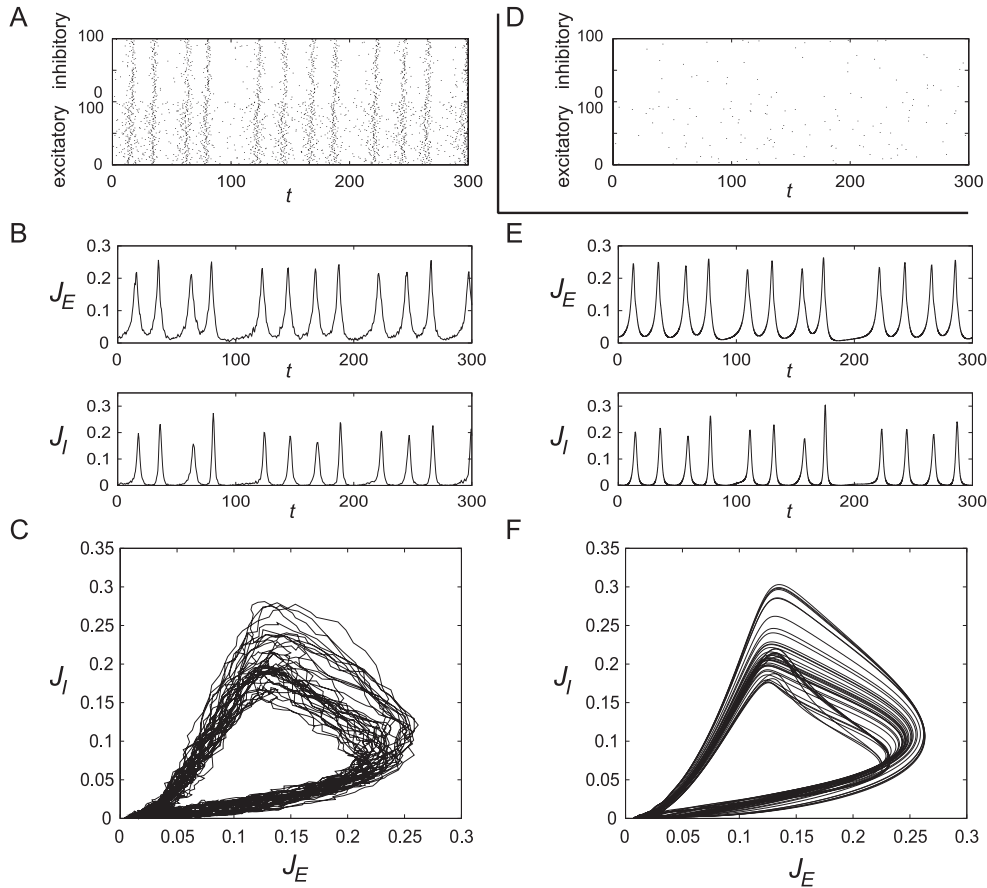
2

Figure 1: (A) Chaotic synchronization observed in a module with $D = 0.0032$, $r_E = r_I = -0.025$, $g_{int} = 4$, and $g_{ext} = 2.5$. Raster plot of spikes of 200 randomly chosen excitatory neurons and inhibitory neurons in a module with $N_E = N_I = 2000$ is shown. (B) Temporal changes in instantaneous firing rates J_E and J_I of the excitatory ensemble and the inhibitory ensemble, respectively, calculated from the data in panel A. (C) Trajectory in the (J_E, J_I) plane. (D) Asynchronous firing observed in this module. Raster plot of spikes of 200 randomly chosen excitatory neurons and inhibitory neurons in a module with $N_E = N_I = 2000$ is shown. (E, F) Chaotic synchronization in a module with an infinite number of neurons obtained by analysis with Fokker-Planck equations. The values of parameters are the same as those used in panels A-D. (E) Temporal changes in the instantaneous firing rates J_E and J_I. (F) Trajectory in the (J_E, J_I) plane.

3 Chaotic pattern alternations observed in multiple modules of network

In this section, we defined a network with multiple modules (Kanamaru, 2007; Kanamaru, Fujii, & Aihara, 2013). Several patterns can be stored in this network according to the mechanism of associative memory and Hebb's rule (Hebb, 1949).

A schematic diagram of the one-module system described in the previous section is shown in Figure 2A. In order to introduce the connections among multiple modules, we analyzed connections from the excitatory ensembles only, as shown in Figure 2B. As indicated below, the strengths of intermodule connections to the excitatory and inhibitory ensembles are scaled by the parameters ϵ_{EE} and ϵ_{IE}, respectively.

The synaptic inputs T_{Ei} and T_{Ii} injected to the ith excitatory ensemble Ei and the inhibitory ensemble Ii, respectively, are defined as

$$T_{Ei} = (g_{int} - \gamma\epsilon_{EE})I_{Ei} - g_{ext}I_{Ii} + \sum_{j=1}^{M}\epsilon_{ij}^{E}I_{Ej} \quad (3.1)$$

$$T_{Ii} = (g_{ext} - \gamma\epsilon_{IE})I_{Ei} - g_{int}I_{Ii} + \sum_{j=1}^{M}\epsilon_{ij}^{I}I_{Ej} \quad (3.2)$$

which are composed of both intra-module and intermodule connections. By replacing the terms $I_E(t)$ and $I_I(t)$ in equations 2.1 and 2.2 with T_{Ei} and T_{Ii} in equations 3.1 and 3.2, a network with multiple modules is defined.
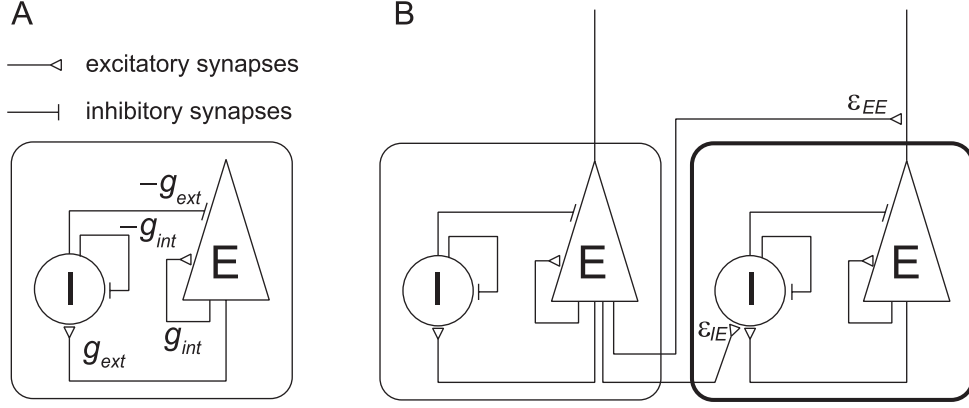
3

Figure 2: (A) A schematic diagram of the one-module system composed of N_E excitatory neurons and N_I inhibitory neurons. (B) A schematic diagram of the connections among multiple modules. Only the connections from excitatory ensembles are considered.

The strengths of connections are defined as

$$\epsilon_{ij}^E = \begin{cases} \epsilon_{EE} K_{ij} & \text{if } K_{ij} > 0 \\ 0 & \text{otherwise} \end{cases}, \qquad (3.3)$$

$$\epsilon_{ij}^I = \epsilon_{IE} |K_{ij}|, \qquad (3.4)$$

$$K_{ij} = \frac{1}{Ma(1-a)} \sum_{\mu=1}^{p} \eta_i^\mu (\eta_j^\mu - a), \qquad (3.5)$$

where $\eta_i^\mu \in \{0, 1\}$ is the stored value in the ith module for the μth pattern, M is the number of modules, p is the number of patterns, and a is the rate of modules that store the value 1. The connection strengths defined by equations 3.3 to 3.5 are used in Kanamaru (2007) and Kanamaru, Fujii, & Aihara (2013) in order to store the patterns composed of 0/1 digits in a pulse neural network. As previously mentioned, ϵ_{EE} and ϵ_{IE} scale the strengths of the intermodule connections to the excitatory and inhibitory ensembles, respectively. In the following, we set $M = 8$, $p = 2$, and $a = 0.5$.

In the associative memory literature, the Hopfield model is well known as a model of the memory retrieval (Hopfield, 1982). In the Hopfield model, an energy function whose local minimum corresponds to each pattern can be defined, and the energy monotonically decreases as the system retrieves the stored pattern successfully. Such dynamics are realized when the connection matrix is symmetric. However, in our model, the connection matrix shown in equation 3.5 is asymmetric; therefore, the energy function cannot be defined in our network.

Typically, memory patterns are thought to be stored during the learning process (Hebb, 1949). In this study, we assume that the patterns have already been stored in the network as attractors before experiments of rivalry, and we called such a set of preexisting attractors as *attractor landscape* (Kanamaru, Fujii, & Aihara, 2013). By showing the patterns to the eyes, some existing attractors that are related to the presented patterns will be activated. It is beyond the scope of this model to know how such attractor landscape was created. Our model examines only the consequences of having particular sorts of attractor landscapes.

Two patterns stored in the network of eight modules are defined as

$$\eta_i^1 = \begin{cases} 1 & \text{if } i \leq M/2 \\ 0 & \text{otherwise} \end{cases}, \qquad (3.6)$$

$$\eta_i^2 = \begin{cases} 1 & \text{if } M/4 < i \leq 3M/4 \\ 0 & \text{otherwise} \end{cases}. \qquad (3.7)$$

In the following, the dynamics of the network are examined by regulating the intermodule connections ϵ_{IE}, for the fixed values of parameters $\gamma = 0.6$ and $\epsilon_{EE} = 1.25$.

Figure 3A reveals that the pattern 1 is successfully retrieved for $\epsilon_{IE} = 1.75$. The changes in the instantaneous firing rates J_{Ei} of the excitatory ensemble in the ith module are aligned vertically. The initial state of the network determines the retrieved pattern.

As shown in Figure 3B, the retrieved pattern alters over time for $\epsilon_{IE} = 1.68$. The analysis of the network is performed with the Fokker-Planck equation, which does not contain noise because the limit $N_E, N_I \to \infty$ is taken. Therefore, the dynamics shown in Figure 3B are not caused by noise but by chaos that is inherent in the network. This fact can be confirmed by analysis using Lyapunov spectra (Kanamaru, 2007).

In order to investigate the retrieved pattern in the network, it is useful to define the overlap of the network with each pattern, which is similar to the inner product (see appendix B). The overlaps m^1 and m^2 with patterns 1 and 2, respectively, are shown in Figure 3C, which have been calculated using the data in Figure 3B. Note that m^i takes values close to 1 when the ith pattern is retrieved.

Moreover, in Figures 3B and 3C, short bursts are observed around $t \simeq 1200, 2500, 15000$, where the modules that store the value 1 in pattern 1 or 2 oscillate. Such patterns are referred to as mixed states in the associative memory literature (Kimoto & Okada, 2001). Although research has revealed several types of mixed states such as OR type or AND type, only the OR type was observed in our network, as shown in Figure 3B.
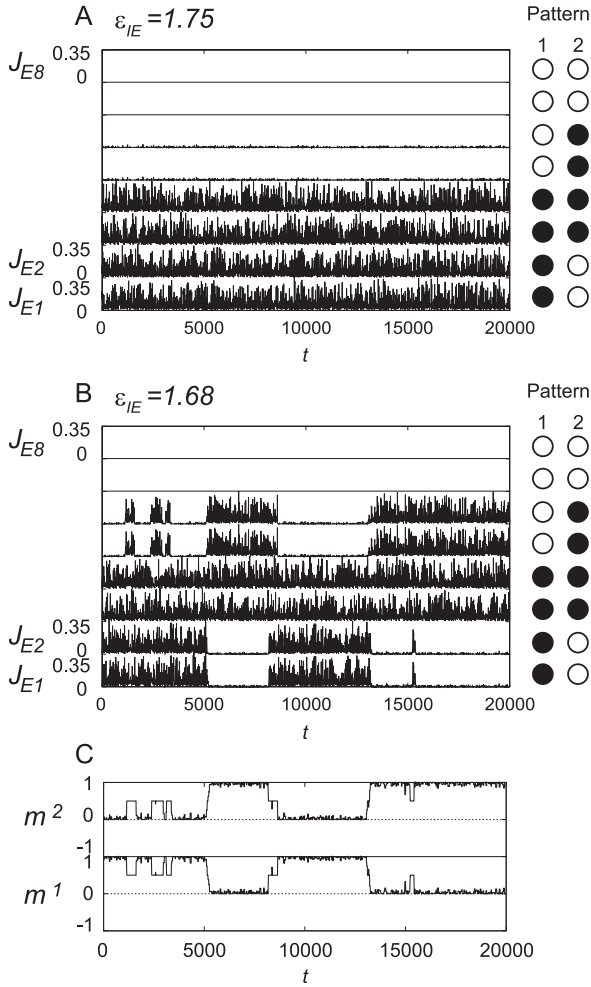
4

Figure 3: (A) Stable pattern retrieval observed in the network of eight modules for $\epsilon_{IE} = 1.75$. Note that pattern 1 is successfully retrieved. (B) Chaotic pattern alternations observed for $\epsilon_{IE} = 1.68$. (C) The overlaps m^1 and m^2 with patterns 1 and 2, respectively.

In order to incorporate the effect of the mixed state into the duration of each pattern, we defined two durations: microscopic and macroscopic. As shown in Figure 4, the mixed state is treated as another pattern in order to examine the microscopic duration. Therefore, the microscopic duration of the pattern $\mu \in \{1, 2\}$ is defined as the duration in which $m^\mu > 0.75$. On the other hand, when examining the macroscopic duration, we regarded that the system retained the previously retrieved pattern even during the period when $0.5 \leq m^1, m^2 < 0.75$.

The macroscopic duration is based on the consideration that the mixed states represent the internal dynamics of the brain and that these states are thus unobservable in psychological experiments. Mixed states were always unstable in the range of ϵ_{IE} in the present study, and their time-averaged duration was much shorter than those of patterns 1 and 2, as we will show.

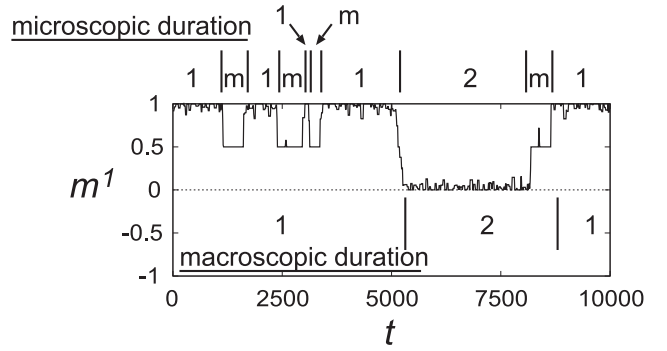In the following, we discuss both the microscopic duration and the macroscopic duration.

Figure 4: The explanation of the microscopic duration and the macroscopic duration.

The dependences of the time-averaged values of the microscopic and macroscopic durations on the intermodule connection strength ϵ_{IE} are shown in Figure 5. All values were calculated using the durations of pattern 1 only, although those of pattern 2 exhibit similar dependence due to the symmetry of the patterns.
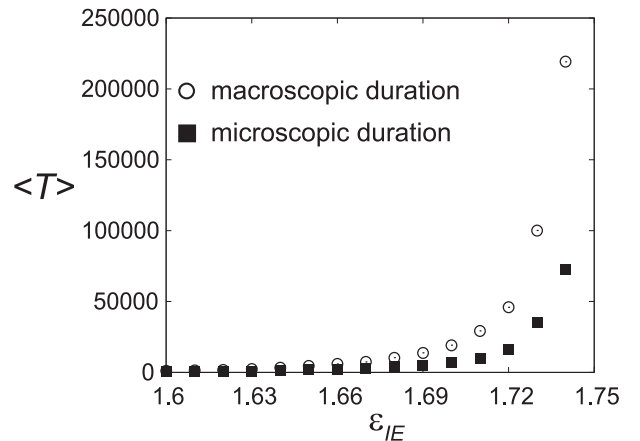

Figure 5: The dependences of time-averaged microscopic durations and macroscopic durations on the intermodule connection strength ϵ_{IE}.

We observed that the time-averaged durations diverged at the critical point $\epsilon_{IE} = \epsilon_0 \simeq 1.75$, and monotonically decreased with decreases in ϵ_{IE}.

The time-averaged durations of the mixed pattern were always below 200 and much shorter than those of patterns 1 and 2 (data not shown).

4   Stochastic properties of pattern durations

In this section, we examine the distribution of the duration of each pattern when chaotic pattern alternations occur.

The distributions of the microscopic durations for $\epsilon_{IE} = 1.6$, 1.64, and 1.68 are shown in Figure 6A. Semi-log plots

of Figure 6A are also shown in Figure 6B. To calculate the distributions, the microscopic durations of both patterns 1 and 2 were used. The solid lines represent the fit with the exponential distribution, and longer durations were associated with better fit. Moreover, for $\epsilon_{IE} = 1.6$, a good fit was observed even for small durations, suggesting that pattern alternations become more stochastic as ϵ_{IE} moves away from the critical point $\epsilon_0 \simeq 1.75$.
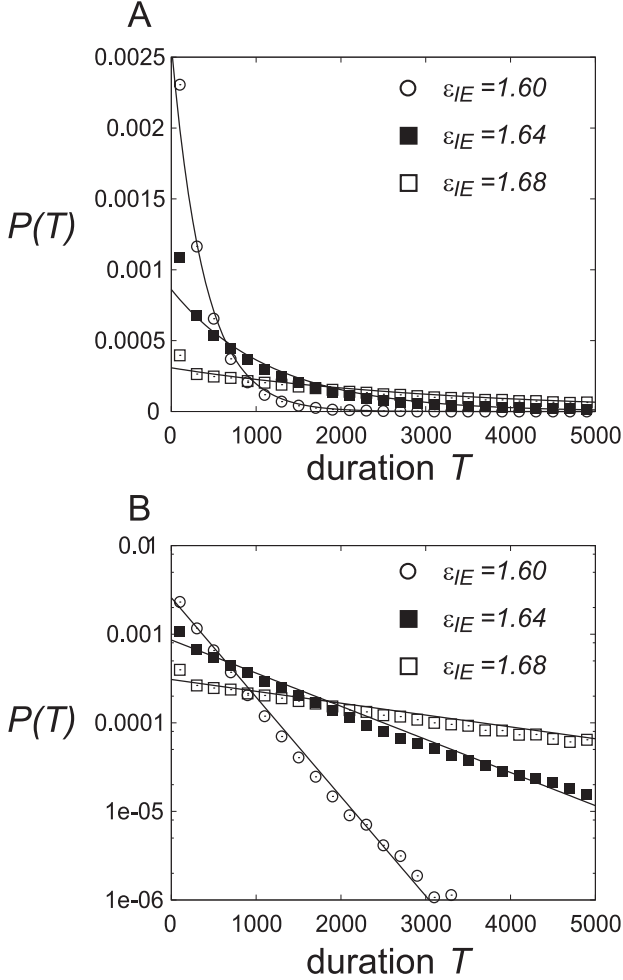

Figure 6: (A) The distribution of the microscopic duration. (B) Semi-log plots of panel A.

The autocorrelation function of the microscopic durations is shown in Figure 7A. The series of microscopic durations is composed by aligning each microscopic duration in order, including the durations of the mixed state. The oscillating component of the autocorrelation function is caused by the fact that the microscopic durations tend to take small values and large values alternately, which correspond to the short durations of the mixed states and the long durations of pattern 1 or 2. In Figure 7A, it is also observed that the oscillating component decreases with the decrease of ϵ_{IE} because the long durations of pattern 1 or 2 decrease and they become comparable to the short durations of the mixed states.

The distributions of the macroscopic durations under identical conditions with Figure 6 are shown in Figure 8. The
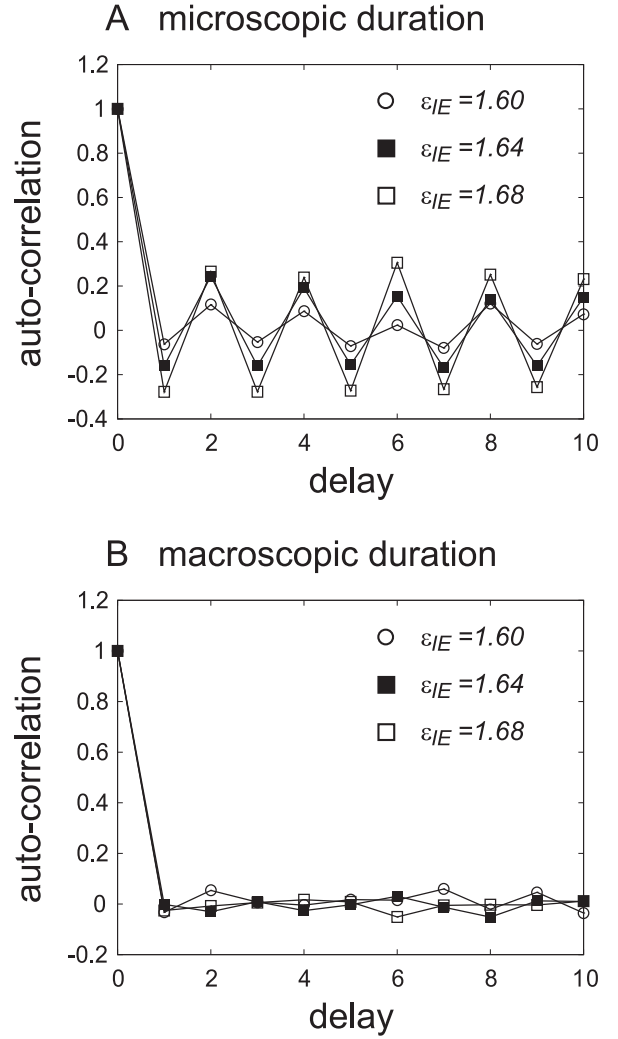

Figure 7: Autocorrelation functions of (A) microscopic durations and (B) macroscopic durations.

solid lines in Figure 8A show the fit with the gamma distribution, and the solid lines in Figure 8B show that with the log-normal distribution.

In Figure 8A, the fit with the gamma distribution $\beta^\alpha T^{\alpha-1} e^{-\beta T} / \Gamma(\alpha)$ is good for $\epsilon_{IE} = 1.6$, where $\Gamma(\alpha)$ is the gamma function with argument α. Note that the fit for large ϵ_{IE} is not good because the decay of the distribution for longer durations is slow for large ϵ_{IE}. This fact also seems to imply that the system with small ϵ_{IE} is more stochastic, as the sum of random variables that obey the exponential distribution obeys the gamma distribution (Murata et al., 2003).

More specifically, the sum of T_i $(i = 1, 2, \cdots, \alpha)$ each of which obeys the exponential distribution with the rate parameter β obeys the gamma distribution with α and β. In Murata et al. (2003), α tended to take natural numbers. The authors proposed that there would be some "distinct states" between two rivalrous states, and the system has to transit such distinct states α times in order to reach the rivalrous states. In our model, the times of passing the mixed states are not fixed but variable (see the data at $t \simeq 2500$ in Figure 4).

6

A gamma distribution
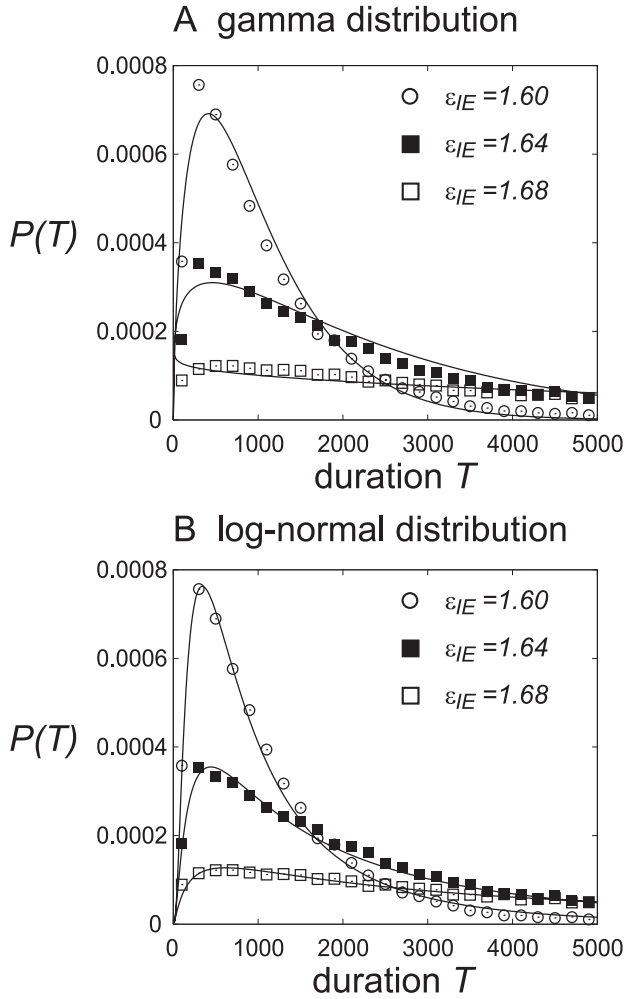

B log-normal distribution

Figure 8: Distributions of the macroscopic durations. (A) The solid lines indicate the fit with the gamma distribution. (B) The solid lines indicate the fit with the log-normal distribution.

It would be interesting to check whether α is a natural number in our model. The parameters (α, β) for gamma distributions in Figure 8A are $(1.66, 0.00158)$, $(1.23, 0.000498)$, and $(0.94, 0.0001)$ for $\epsilon_{IE} = 1.60$, 1.64, and 1.68, respectively. The parameter value $\alpha = 1.66$ for $\epsilon_{IE} = 1.60$ seems to indicate that both the direct transition to another pattern ($\alpha = 1$) and the transition passing the mixed pattern once ($\alpha = 2$) exist.

In Lehky (1995), the dominant durations of binocular rivalry follow a log-normal distribution. Similarly, the distribution of the macroscopic durations in our system also follows a log-normal distribution, as shown in Figure 8B.

The autocorrelation function of the macroscopic durations is shown in Figure 7B. The series of macroscopic durations is composed by aligning the macroscopic durations of pattern 1 and pattern 2 in order. The autocorrelation function indicates that the macroscopic durations do not have any sequential dependence, which is consistent with psychological experiments (Walker, 1975).

In summary, the macroscopic durations are more appropriate than microscopic durations as models of the dominance durations of binocular rivalry and perceptual ambiguity.

5 Peak position of the distribution

Previous psychological research has revealed that the dominance duration that gives the peak of the distribution ranges from 0.8 s to 10 s, depending on the individual participant (Levelt, 1967; Borsellino et al., 1972; Walker, 1975; Lehky, 1995; Blake, 2001). In this section, we examine the origin of this variability of the peak position T_p.

First, careful observation of Figure 8 shows that T_p slightly depends on the intermodule connection strength ϵ_{IE}. Second, it is expected that T_p would become large when the number of the mixed states increases because the network will pass many mixed states before it moves from one pattern to another. To confirm this expectation, we add the third pattern to the network by setting the number of patterns $p = 3$ in equation 3.5 and defining the third pattern as

$$\eta_i^3 = \begin{cases} 1 & \text{if } i \bmod 2 = 1 \\ 0 & \text{otherwise} \end{cases}. \qquad (5.1)$$

As shown in Figure 9, the number of mixed states are six for $p = 3$. Similarly to the case with $p = 2$, we define the macroscopic duration of the μth pattern as the time during which $m^\mu \geq 0.5$ is satisfied.

The dependences of T_p on the intermodule connection strength ϵ_{IE} in the network with $p = 2$ and $p = 3$ are shown in Figure 10, which is calculated for the fit with the log-normal distribution of the macroscopic durations.
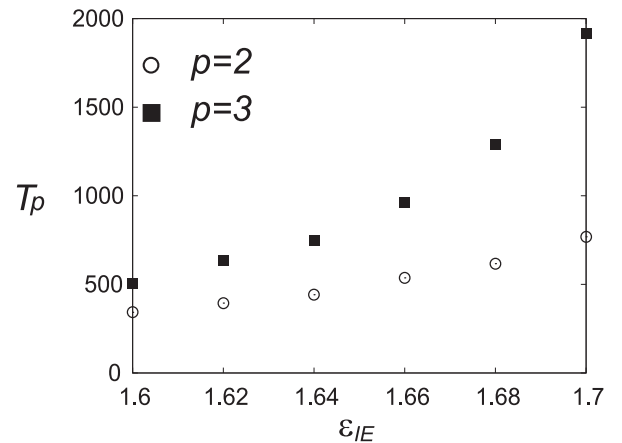

Figure 10: The dependences of the macroscopic duration T_p that gives the peak of distribution on ϵ_{IE} in the networks with $p = 2$ and $p = 3$.

It is observed that T_p in the network with $p = 3$ is larger than that in the network with $p = 2$. Moreover, for both $p = 2$ and $p = 3$, it is observed that T_p increases with the increase of ϵ_{IE}.
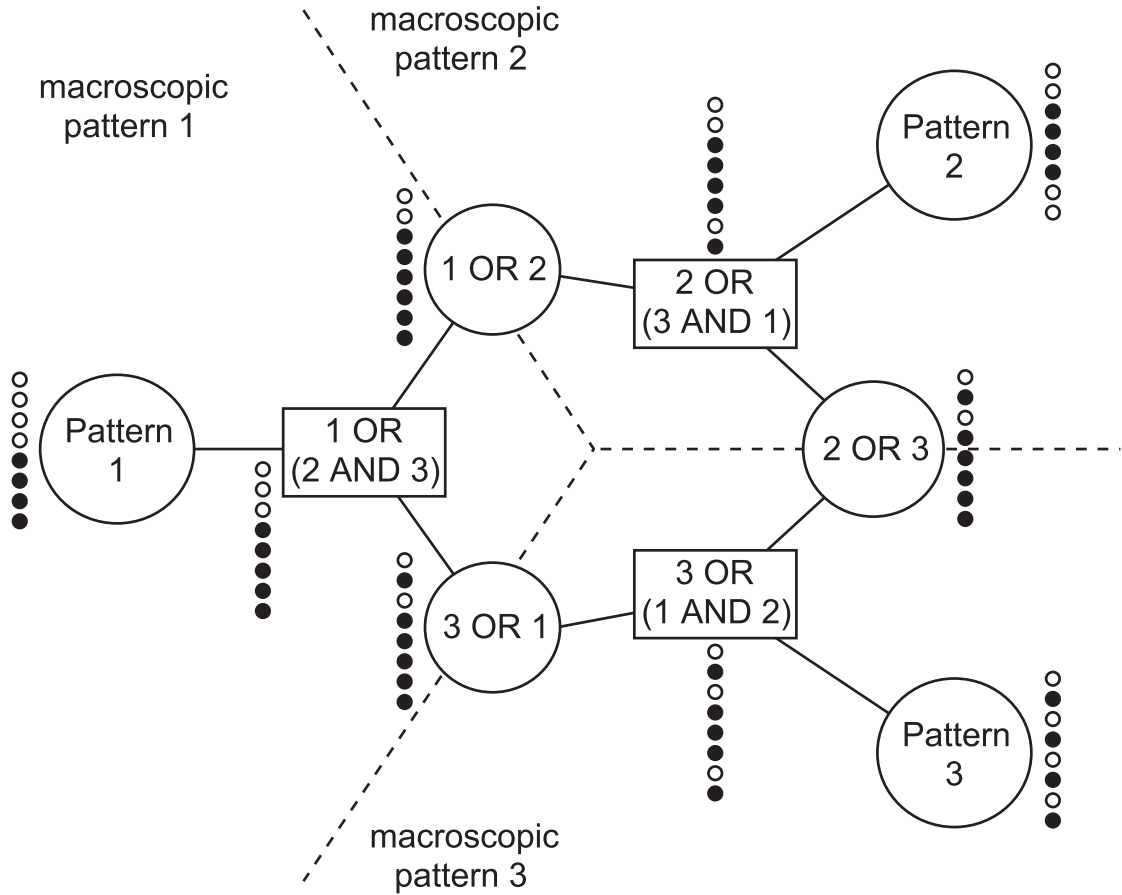
Figure 9: The relationships among three patterns and their mixed states.

6 Chaotic properties of pattern durations

Lehky (1995) reports that the series of dominance durations is not chaotic. In this section, we examine the chaotic properties of the chaotic pattern alternations.

In order to examine the chaotic properties of the series of dominance durations, Lehky (1995) used the correlation dimension and the time series prediction based on reconstruction. Moreover, Lehky also used the surrogate data of the original data when calculating the correlation dimension and the time series prediction error to discriminate chaos and stochastic processes (Theiler et al., 1992).

In this study, we use only the time series prediction based on reconstruction for the original and surrogate data, because it is known that calculating correlation dimension requires a large number of data to obtain reliable results (Smith, 1988; Ruelle, 1990). Although Lehky (1995) examined the dependence of the time series prediction error on the embedding dimension, we examine its dependence on the prediction step to check the existence of the sensitive dependence on the initial conditions that is typical of chaos (Kanamaru & Sekine, 2005a).

Although we examine only the network with $p = 2$, similar results are observed also in the network with $p = 3$.

In the time series prediction based on reconstruction (detailed in appendix C), some surrogate data are generated from the original time series under certain null hypotheses so that the new time series preserve some statistical properties of the original data. In the study presented in this letter, we used two types of surrogates, random shuffled (RS) and amplitude adjusted Fourier transformed (AAFT) surrogate data, which correspond to the null hypothesis of an independent and identically distributed random process and that of a linear stochastic process observed through a monotonic nonlinear function, respectively.

We then calculated the nonlinear prediction error $E_{NP}(h)$ for the prediction step h for both the original and surrogate data. If $E_{NP}(h)$ for the surrogate data is significantly different from that of the original data, the null hypothesis is rejected, and it can be concluded that there is some possibility that the original time series has deterministic properties, such as strange attractors. On the other hand, if $E_{NP}(h)$ for the surrogate data exhibits no significant difference from that of the original data, the null hypothesis is not rejected, and the original data can be regarded as being generated from some stochastic process.

$E_{NP}(h)$ for the microscopic durations is shown in Figures 11A and 11B. The examined time series $\{T_i\}$ is identical to that used in Figure 7A. As shown in Figure 11A, for
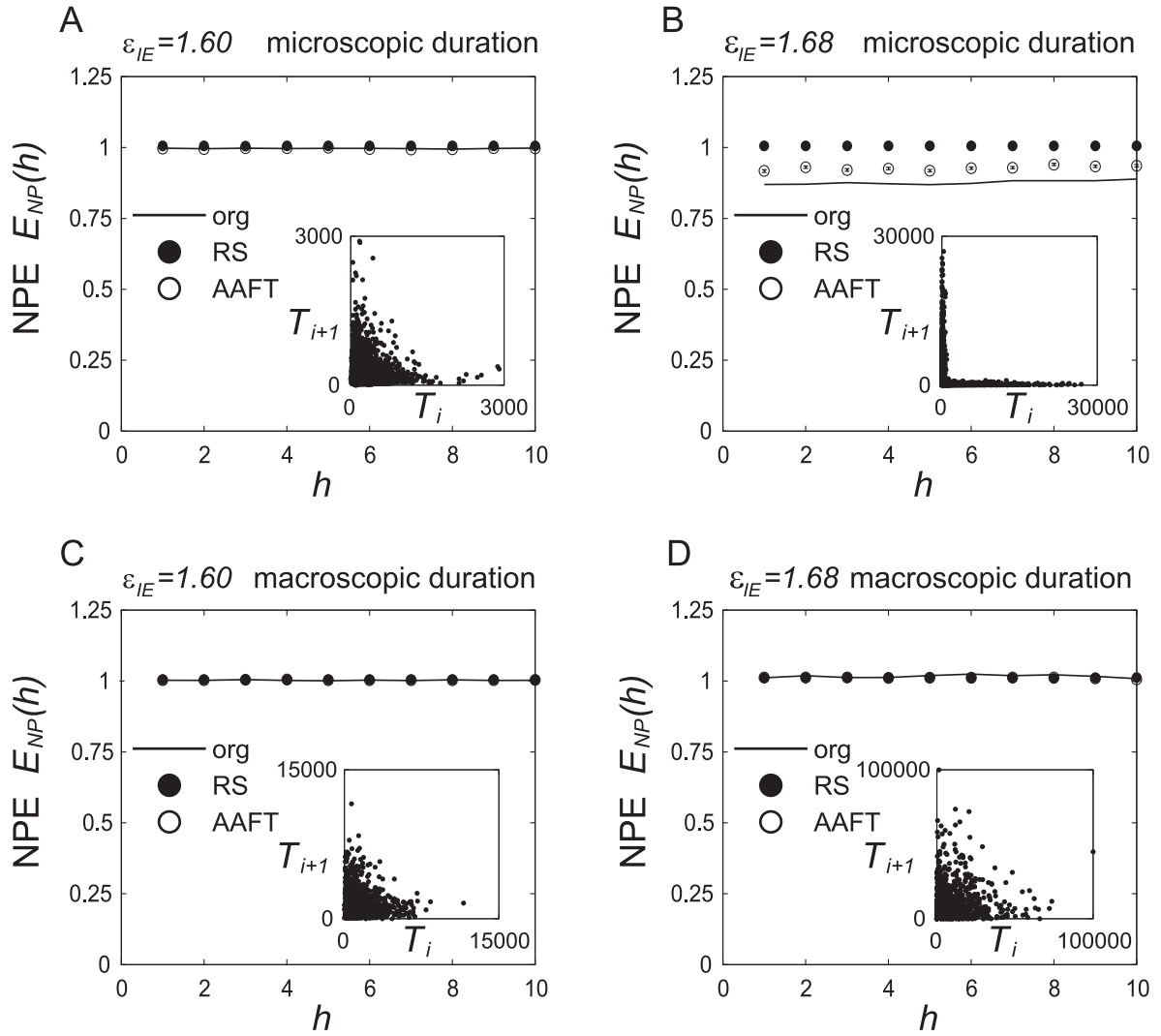
8

Figure 11: The dependence of the nonlinear prediction error $E_{NP}(h)$ on prediction step h for the time series of (A, B) the microscopic durations, and (C, D) the macroscopic durations. The return plots of $\{T_i\}$ in the (T_i, T_{i+1}) plane are also shown in the insets. In panels A, C, and D, $E_{NP}(h)$ of the RS and AAFT surrogate data are not significantly different from those of the original data. In panel B, $E_{NP}(h)$ of the RS and AAFT surrogate data are significantly different from those of the original data, although this is due to alternations between small values and large values.

$\epsilon_{IE} = 1.6$, $E_{NP}(h)$ of the RS and AAFT surrogate data exhibit no significant difference from those of the original data. Therefore, the time series of microscopic durations for $\epsilon_{IE} = 1.6$ is regarded as being generated by some stochastic process. This finding supports our previous observation that the microscopic durations for $\epsilon_{IE} = 1.6$ seem to be stochastic. We also observed no deterministic structures in the return plot of the time series $\{T_i\}$.

As shown in Figure 11B, for $\epsilon_{IE} = 1.68$, $E_{NP}(h)$ of the RS and AAFT surrogate data exhibit significant differences from those of the original data. This finding suggests that there are some deterministic structures in the original time series $\{T_i\}$, but that such deterministic structures are not caused by chaos for two reasons. First, if there is chaos in the time series, the nonlinear prediction error $E_{NP}(h)$ would increase with increases in the prediction step h because of

the sensitive dependence on the initial condition. However, $E_{NP}(h)$ is almost constant, as shown in Figure 11B. Second, the return plot of $\{T_i\}$ in the inset reveals that $\{T_i\}$ tends to take small values and large values alternately. This tendency is also observed in Figure 7A. This property makes the prediction easier, producing small values of $E_{NP}(h)$. Therefore, we conclude that chaos is not observed in the time series $\{T_i\}$ for $\epsilon_{IE} = 1.68$.

We performed similar analyses for macroscopic durations, the results of which are presented in Figures 11C and 11D. The examined time series $\{T_i\}$ is identical to that used in Figure 7B. The nonlinear prediction errors $E_{NP}(h)$ for $\epsilon_{IE} = 1.6$ and 1.68 did not significantly differ from those of the original data. Therefore, the time series $\{T_i\}$ are regarded as being generated by some stochastic process.

In summary, chaotic properties are not observed in the

time series of either microscopic or macroscopic durations. This result suggests that our model is consistent with the results in Lehky (1995).

7 Two properties of the binocular rivalry

In this section, we show that our model can reproduce two characteristics of binocular rivalry.

First, when reducing the contrast of a stimulus to one eye, it is known that dominance intervals in the other eye increase and dominance intervals in the stimulated eye are relatively unchanged (Laing & Chow, 2002; Wilson, 2007).

To reproduce this observation, in the network with $p = 2$, we reduce the contrast of pattern 1, and we observe the mean macroscopic durations $\langle T^{(1)} \rangle$ and $\langle T^{(2)} \rangle$ of patterns 1 and 2, respectively. The contrast of pattern 1 is defined as the strength of the the constant inputs to the modules that store the value 1 for pattern 1. For that purpose, we replace the parameter r_E of the modules that store the value 1 for pattern 1 with $r_E + dr_E^{(1)}$.

The dependences of $\langle T^{(1)} \rangle$ and $\langle T^{(2)} \rangle$ on $dr_E^{(1)}$ for three values of ϵ_{IE} are shown in Figure 12A. It is observed that $\langle T^{(2)} \rangle$ mainly increases and $\langle T^{(1)} \rangle$ moderately decreases when decreasing $dr_E^{(1)}$. Note that the data are not shown when $\langle T^{(2)} \rangle$ diverges for $\epsilon_{IE} = 1.68$.

Second, we show that dominance intervals in both eyes decreases when increasing the contrast of the stimuli to both eyes (Laing & Chow, 2002; Wilson, 2007). For that purpose, we replace the parameter r_E of the modules that store the value 1 for pattern 1 or 2 with $r_E + dr_E^{(1,2)}$.

The dependences of $\langle T^{(1)} \rangle$ and $\langle T^{(2)} \rangle$ on $dr_E^{(1,2)}$ are shown in Figure 12B. It is observed that both $\langle T^{(1)} \rangle$ and $\langle T^{(2)} \rangle$ tend to decrease with the increase of $dr_E^{(1,2)}$ for three values of ϵ_{IE}. Although fluctuation in $\langle T^{(1)} \rangle$ and $\langle T^{(2)} \rangle$ is large for $\epsilon_{IE} = 1.68$, it might be because some bifurcations take place in this range of $dr_E^{(1,2)}$; however, the tendency for $\langle T^{(1)} \rangle$ and $\langle T^{(2)} \rangle$ to decrease is still observed.

8 Conclusions

We proposed a pulse neural network that exhibits chaotic pattern alternations between two stored patterns as a model of multistable perception, which is reflected in such phenomena as binocular rivalry and perceptual ambiguity.

To measure the durations of each pattern, we introduced two durations. The microscopic durations treated the mixed state as another pattern, while the macroscopic durations treated the mixed state as part of each pattern.

The distribution of the microscopic durations was characterized by a monotonically decreasing function and followed an exponential distribution for large durations. On the other hand, the distribution of the macroscopic durations was unimodal, following a gamma or log-normal distribution, though the log-normal distribution was associated with
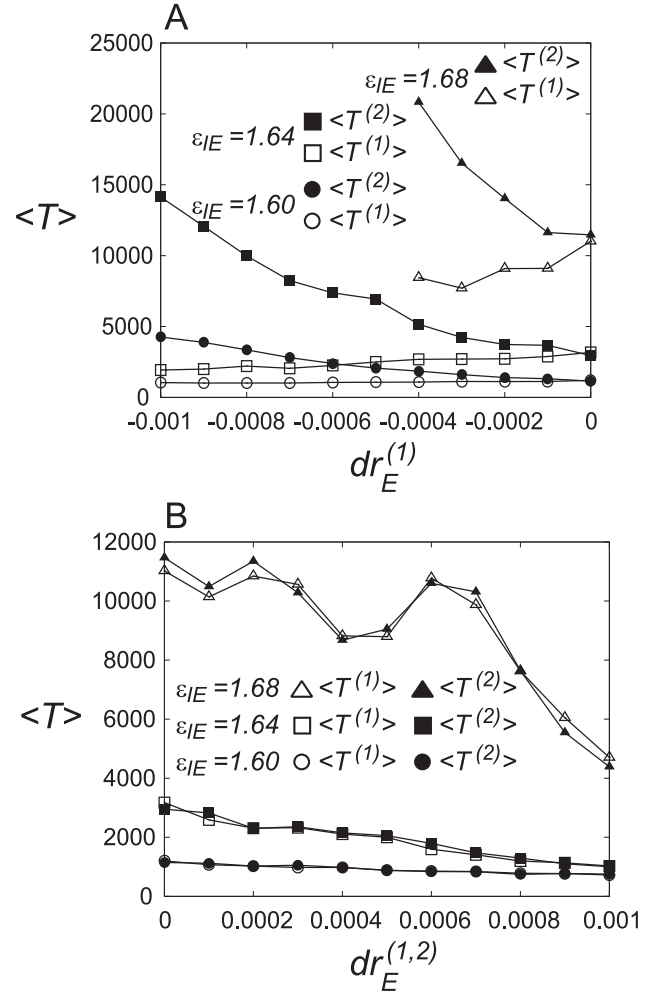

Figure 12: Two characteristics of binocular rivalry. (A) When reducing the contrast $dr_E^{(1)}$ of pattern 1, the mean macroscopic duration $\langle T^{(2)} \rangle$ of pattern 2 increases and the mean macroscopic duration $\langle T^{(1)} \rangle$ of pattern 1 is relatively unchanged. (B) When increasing the contrast $dr_E^{(1,2)}$ of both patterns, the mean macroscopic durations $\langle T^{(1)} \rangle$ and $\langle T^{(2)} \rangle$ of both patterns tend to decrease.

improved fit relative to the gamma distribution. Therefore, we conclude that the macroscopic durations of the chaotic pattern alternations can reproduce the unimodal distribution of dominance durations observed in multistable perception. It is found that the peak position of the distribution depends on the number of mixed patterns and intermodule connection strength.

Moreover, we examined the existence of chaotic properties in the time series of durations using a time series prediction method based on reconstruction. The results of our analysis revealed no chaotic properties for either duration. Therefore, our model is consistent with the previous finding that the dominance durations of binocular rivalry are not chaotic, as Lehky (1995) stated.

It was also shown that our model can reproduce two characteristics of binocular rivalry. First, when reducing the con-

trast of a stimulus to one eye, dominance intervals in the other eye increase and dominance intervals in the stimulated eye are relatively unchanged (Laing & Chow, 2002; Wilson, 2007). Second, when increasing the contrast of the stimuli to both eyes, dominance intervals in both eyes decrease (Laing & Chow, 2002; Wilson, 2007).

In summary, our network with chaotic pattern alternations can be regarded as a model of multistable perception.

The absence of chaotic properties in the durations of chaotic pattern alternations may be due to several reasons. First, the durations are much longer than the time scale of the chaotic oscillations. For example, the inter-peak intervals of the chaotic oscillations in Figure 1E are approximately $\Delta t \simeq 25$. If we analyze the chaotic properties in the time series of these inter-peak intervals, chaos is observed (Kanamaru & Sekine, 2005a). However, the durations of chaotic pattern alternations are much longer than those in Figure 3B; therefore, chaos was not observed. This property reflects the fact that our network is composed of pulse neurons and uses chaotic synchronization. Second, the absence of chaos may be related to aspects of chaos theory, which states that in a system under crisis, the durations of the system that remains around the destabilized chaotic attractor obey the exponential distribution, and they have a sensitive dependence on the initial conditions (Ott, 2002). In our model, the durations obeying the exponential distributions correspond to the results in Figure 6. The sensitive dependence of the durations on the initial conditions implies that the time series of the durations become stochastically independent, and in our model, this fact corresponds to the results in Figures 7, 11A, and 11B. The oscillating component in Figure 7A and the deterministic properties in Figure 11B are caused by the tendency to take small values and large values alternatively, and they are not related to chaos; such deterministic properties disappear when the macroscopic durations are used as shown in Figures 7B and 11D.

Finally, we state the difference between our model and Nagao's chaotic associative memory model (Nagao et al., 2000). First, Nagao's model is composed of conventional neuronal models based on firing rates, and our model is composed of the pulse neurons. Second, the used patterns have different structures. Nagao et al.'s model uses two patterns made by perturbing an original pattern; therefore, their patterns are correlated with each other, while our patterns are orthogonal to each other. Their unperturbed original patterns would correspond to our mixed states. The reason why our model can reproduce the unimodal distribution of the dominance duration without the unperturbed pattern would be because our pattern is composed of 0/1 digits, while Nagao's model uses $-1/1$ digits. In order to store the patterns composed of 0/1 digits into a pulse neural network, we used connection strengths defined by equations 3.3 to 3.5 that were modified from the original Hebb rule (Kanamaru, 2007). With such modified connection strengths, our model can easily increase the number of mixed states by increasing the number of stored patterns, and by this fact, the peak position of the distribution of the dominance duration can be changed as shown in Figure 10.

A Fokker-Planck equation

To analyze the average dynamics of the one-module system, we used the Fokker-Planck equations (Gerstner & Kistler, 2002), which are written as

$$
\begin{aligned}
\frac{\partial n_E}{\partial t} &= -\frac{\partial}{\partial \theta_E}(A_E n_E) \\
&\quad + \frac{D}{2}\frac{\partial}{\partial \theta_E}\left\{ B_E \frac{\partial}{\partial \theta_E}(B_E n_E) \right\}, \quad \text{(A.1)}
\end{aligned}
$$

$$
\begin{aligned}
\frac{\partial n_I}{\partial t} &= -\frac{\partial}{\partial \theta_I}(A_I n_I) \\
&\quad + \frac{D}{2}\frac{\partial}{\partial \theta_I}\left\{ B_I \frac{\partial}{\partial \theta_I}(B_I n_I) \right\}, \quad \text{(A.2)}
\end{aligned}
$$

$$
\begin{aligned}
A_E(\theta_E, t) &= (1 - \cos\theta_E) + (1 + \cos\theta_E) \\
&\quad \times (r_E + g_{int}I_E(t) - g_{ext}I_I(t)), \text{(A.3)}
\end{aligned}
$$

$$
\begin{aligned}
A_I(\theta_I, t) &= (1 - \cos\theta_I) + (1 + \cos\theta_I) \\
&\quad \times (r_I + g_{ext}I_E(t) - g_{int}I_I(t)), \text{(A.4)}
\end{aligned}
$$

$$
B_E(\theta_E, t) = 1 + \cos\theta_E, \quad \text{(A.5)}
$$

$$
B_I(\theta_I, t) = 1 + \cos\theta_I, \quad \text{(A.6)}
$$

for the normalized number densities of excitatory and inhibitory ensembles, in which

$$
n_E(\theta_E, t) \equiv \frac{1}{N_E}\sum \delta(\theta_E^{(i)} - \theta_E), \quad \text{(A.7)}
$$

$$
n_I(\theta_I, t) \equiv \frac{1}{N_I}\sum \delta(\theta_I^{(i)} - \theta_I), \quad \text{(A.8)}
$$

in the limit of $N_E, N_I \to \infty$. The probability flux for each ensemble is defined as

$$
J_E(\theta_E, t) = A_E n_E - \frac{D}{2}B_E \frac{\partial}{\partial \theta_E}(B_E n_E), \quad \text{(A.9)}
$$

$$
J_I(\theta_I, t) = A_I n_I - \frac{D}{2}B_I \frac{\partial}{\partial \theta_I}(B_I n_I), \quad \text{(A.10)}
$$

respectively. The probability flux at $\theta = \pi$ can be interpreted as the instantaneous firing rate in this ensemble, which is denoted as $J_X(t) \equiv J_X(\pi, t)$ where $X = E$ or I.

$I_X(t)$ in equation 2.3 follows a differential equation that is written as

$$
\dot{I_X}(t) = -\frac{1}{\kappa_X}\left(I_X(t) - \frac{1}{2}J_X(t) \right). \quad \text{(A.11)}
$$

In order to integrate the Fokker-Planck equations (A.1) and (A.2) numerically, we expanded $n_E(\theta_E, t)$ and $n_I(\theta_I, t)$ into Fourier series as

$$
\begin{aligned}
n_E(\theta_E, t) &= \frac{1}{2\pi} \\
&+ \sum_{k=1}^{\infty}(a_k^E(t)\cos(k\theta_E) + b_k^E(t)\sin(k\theta_E)), \text{(A.12)}
\end{aligned}
$$

$$
\begin{aligned}
n_I(\theta_I, t) &= \frac{1}{2\pi} \\
&+ \sum_{k=1}^{\infty}(a_k^I(t)\cos(k\theta_I) + b_k^I(t)\sin(k\theta_I)), \quad \text{(A.13)}
\end{aligned}
$$

and, by substituting them, equations A.1 and A.2 were transformed into a set of ordinary differential equations of a_k^X and b_k^X, which are written as

$$\frac{da_k^{(X)}}{dt} = -(r_X + \tilde{I}_X + 1)kb_k^{(X)}$$
$$-(r_X + \tilde{I}_X - 1)\frac{k}{2}(b_{k-1}^{(X)} + b_{k+1}^{(X)})$$
$$-\frac{Dk}{8}g(a_k^{(X)}), \qquad (A.14)$$

$$\frac{db_k^{(X)}}{dt} = (r_X + \tilde{I}_X + 1)ka_k^{(X)}$$
$$+(r_X + \tilde{I}_X - 1)\frac{k}{2}(a_{k-1}^{(X)} + a_{k+1}^{(X)})$$
$$-\frac{Dk}{8}g(b_k^{(X)}) \qquad (A.15)$$

$$g(x_k) = (k-1)x_{k-2} + 2(2k-1)x_{k-1} + 6kx_k$$
$$+2(2k+1)x_{k+1} + (k+1)x_{k+2}, \quad (A.16)$$

$$\tilde{I}_E \equiv g_{int}I_E - g_{ext}I_I, \qquad (A.17)$$
$$\tilde{I}_I \equiv g_{ext}I_E - g_{int}I_I, \qquad (A.18)$$
$$a_0^{(X)} \equiv \frac{1}{\pi}, \qquad (A.19)$$
$$b_0^{(X)} \equiv 0, \qquad (A.20)$$

where $X = E$ or I. By integrating the ordinary differential equations (A.11), (A.14), and (A.15) numerically, the time series of the probability fluxes J_E and J_I are obtained. For numerical calculations, each Fourier series was truncated at the first 40 terms.

B Definition of overlap

In this section, we provide a method for calculating the overlap m^μ between a set of instantaneous firing rates J_{Ei} of excitatory neurons in a module ($1 \le i \le M$) and the stored pattern η_i^μ.

Because J_{Ei} is an oscillating quantity, the overlap of the usual definition is also oscillating, even when the correct pattern is retrieved. To obtain an overlap that maintains an almost constant value when the correct pattern is retrieved, we defined a peak-value function $P_{Ei}(t)$ as $P_{Ei}(t) = J_{Ei}(t^*)$, where t^* is the nearest time point that gives a peak of $J_{Ei}(t)$ and satisfies $t^* < t$. We then transformed $P_{Ei}(t)$ to function $O_{Ei}(t)$ with a range of [0,1]:

$$O_{Ei}(t) = \begin{cases} 1 & (P_{Ei}(t) > \theta_2) \\ \frac{P_{Ei}(t) - \theta_1}{\theta_2 - \theta_1} & (\theta_1 \le P_{Ei}(t) \le \theta_2) \\ 0 & (P_{Ei}(t) < \theta_1) \end{cases} , \quad (B.1)$$

where $\theta_1 = 0.01$ and $\theta_2 = 0.1$. Using $O_{Ei}(t)$, the overlap m^μ between the state of the network and the stored pattern

η_i^μ is defined as

$$m^\mu = \frac{1}{Ma(1-a)}\sum_{i=1}^{M}(\eta_i^\mu - a)(O_{Ei} - a), \quad (B.2)$$
$$= \frac{1}{Ma(1-a)}\sum_{i=1}^{M}(\eta_i^\mu - a)O_{Ei}. \qquad (B.3)$$

C Nonlinear prediction based on reconstruction

In this section, the nonlinear prediction method based on reconstruction of dynamics is summarized (Theiler et al., 1992; Sauer, 1994).

Let us consider a sequence $\{T_k\}$ of the duration of patterns and the delay coordinate vectors $V_j = (T_{j-m+1}, T_{j-m+2}, \ldots, T_j)$ with the reconstruction dimension m, and let L be the number of vectors in the reconstructed phase space $\mathbf{R}^m$. For a fixed integer j_0, we chose $l = \beta L$ ($\beta < 1$) points that are nearest to the point V_{j_0} and denoted them by $V_{j_k} = (T_{j_k-m+1}, T_{j_k-m+2}, \ldots, T_{j_k})(k = 1, 2, \ldots, l)$. With $\{V_{j_k}\}$, a predictor of T_{j_0} for h steps ahead is defined as

$$p_{j_0}(h) = \frac{1}{l}\sum_{k=1}^{l}T_{j_k+h}. \qquad (C.1)$$

With $p_{j_0}(h)$, the normalized prediction error (NPE) is defined as

$$E_{NP}(h) = \frac{\langle(p_{j_0}(h) - T_{j_0+h})^2\rangle^{1/2}}{\langle(\langle T_{j_0}\rangle - T_{j_0+h})^2\rangle^{1/2}}, \qquad (C.2)$$

where $\langle\cdot\rangle$ denotes the average over j_0. A small value of NPE $i.e.$, less than 1, implies that the sequence has deterministic structure behind the time series because this algorithm is based on the assumption that the dynamical structure of a finite-dimensional deterministic system can be well reconstructed by the delay coordinates of the sequence (Sauer, 1994). However, stochastic time series with large autocorrelations can also take NPE values less than 1. Therefore, we could not conclude that there is deterministic structure only from the magnitude of NPE.

To confirm the deterministic structure, the values of NPE should be compared with those of NPE for a set of surrogate data (Theiler et al., 1992). The surrogate data used in the present study were new time series generated from the original time series under some null hypotheses so that the new time series preserve some statistical properties of the original data. In the present study, we used random shuffled (RS) and amplitude adjusted Fourier transformed (AAFT) surrogate data, which correspond to the null hypothesis of an independent and identically distributed random process and that of a linear stochastic process observed through a monotonic nonlinear function, respectively. To obtain AAFT surrogate data, we used TISEAN 3.0.1 (Hegger, Kantz, & Schreiber, 1999; Schreiber & Schmitz, 2000). If the values of NPE for the original data are significantly smaller than those of NPE

for the surrogate data, the null hypothesis is rejected, and it can be concluded that there is some possibility that the original time series has deterministic structure.

References

Adachi, M., & Aihara, K. (1997). Associative dynamics in a chaotic neural network. *Neural Networks*, *10*, 83 – 98.

Aihara, K., Takabe, T., & Toyoda, M. (1990). Chaotic neural networks. *Physics Letters A*, *144*, 333 – 340.

Alais, D., & Blake, R. (2015). Binocular rivalry and perceptual ambiguity. In J. Wagemans (Eds.), *The Oxford Handbook of Perceptual Organization*, Oxford University Press.

Blake, R. (2001). A primer on binocular rivalry, including current controversies. *Brain and Mind*, *2*, 5 – 38.

Borsellino, A., Marco, A. De, Alliazetta, A., Rinesi, S., & Bartolini, B. (1972). Reversal time distribution in the perception of visual ambiguous stimuli. *Kybernetik*, *10*, 139 – 144.

Ermentrout, B. (1996). Type I membranes, phase resetting curves, and synchrony. *Neural Computation*, *8*, 979 – 1001.

Ermentrout, G. B., & Kopell, N. (1986). Parabolic bursting in an excitable system coupled with a slow oscillation. *SIAM Journal on Applied Mathematics*, *46*, 233 – 253.

Freeman, A. W. (2005). Multistage model for binocular rivalry. *Journal of Nueorophysiology*, *94*, 4412 – 4420.

Gerstner, W., & Kistler, W. (2002). *Spiking Neuron Models.* Cambridge: Cambridge Univ. Press.

Hebb, D. O. (1949). *The Organization of Behavior – a neuropsychological theory.* New York: John Wiley.

Hegger, R., Kantz, H., & Schreiber, T. (1999). Practical implementation of nonlinear time series methods: The TISEAN package. *Chaos*, *9*, 413 – 435.

Hopfield, J. J. (1982). Neural networks and physical systems with emergent collective computational properties. *Proc. Nat. Acad. Sci. (USA)*, *79*, 2554 – 2558.

Inoue, M., & Nagayoshi, A. (1991). A chaos neurocomputer. *Physics Letters A*, *158*, 373 – 376.

Izhikevich, E. M. (1999). Class 1 neural excitability, conventional synapses, weakly connected networks, and mathematical foundations of pulse-coupled models. *IEEE Transactions on Neural Networks*, *10*, 499 – 507.

Izhikevich, E. M. (2000). Neural excitability, spiking and bursting. *International Journal of Bifurcation and Chaos*, *10*, 1171 – 1266.

Kanamaru, T. (2007). Chaotic pattern transitions in pulse neural networks. *Neural Networks*, *20*, 781 – 790.

Kanamaru, T., Fujii, H., & Aihara, K. (2013). Deformation of attractor landscape via cholinergic presynaptic modulations: A computational study using a phase neuron model. *PLOS ONE*, *8*, e53854.

Kanamaru, T., & Sekine, M. (2005a). Detecting chaotic structures in noisy pulse trains based on interspike interval reconstruction. *Biological Cybernetics*, *92*, 333 – 338.

Kanamaru, T., & Sekine, M. (2005b). Synchronized firings in the networks of class 1 excitable neurons with excitatory and inhibitory connections and their dependences on the forms of interactions. *Neural Computation*, *17*, 1315-1338.

Kimoto, T., & Okada, M. (2001). Mixed state on a sparsely encoded associative memory model. *Biological Cybernetics*, *85*, 319 – 325.

Laing, C. R., & Chow, C. C. (2002). A spiking neuron model for binocular rivalry. *Journal of Computational Neuroscience*, *12*, 39 – 53.

van Leeuwen, C., Steyvers, M., & Nooter, M. (1997). Stability and intermittency in large-scale coupled oscillator models for perceptual segmentation. *Journal of Mathematical Psychology*, *41*, 319 – 344.

Lehky, S. R. (1988). An astable multivibrator model of binocular rivalry. *Perception*, *17*, 215 – 228.

Lehky, S. R. (1995). Binocular rivalry is not chaotic. *Proceedings of the Royal Society of London B*, *259*, 71 – 76.

Levelt, W. J. M. (1967). Note on the distribution of dominance times in binocular rivalry. *British Journal of Psychology*, *58*, 143 – 145.

Logothestis, N. K., Leopold, D. A., & Sheinberg, D. L. (1996). What is rivalling during binocular rivalry? *Nature*, *380*, 621 – 624.

Murata, T., Matsui, N, Miyauchi, S., Kakita, Y., & Yanagida, T. (2003). Discrete stochastic process underlying perceptual rivalry. *Neuroreport*, *14*, 1347 – 1352..

Nagao, N., Nishimura, H., & Matsui, N. (2000). A neural chaos model of multistable perception. *Neural Processing Letters*, *12*, 267 – 276.

Nara, S., & Davis, P. (1992). Chaotic wandering and search in a cycle-memory neural network. *Progress of Theoretical Physics*, *88*, 845 – 855.

Ott, E. (2002). *Chaos in Dynamical Systems.* (2nd ed.). New York: Cambridge University Press.

Ruelle, D. (1990). The Claude Bernard lecture, 1989. Deterministic chaos: the science and the fiction. *Proc. R. Soc. Lond. A*, *427*, 241 – 248.

Sauer, T. (1994). Reconstruction of dynamical systems from interspike interval. *Rhys. Rev. Lett*, *72*, 3811 – 3814.

Schreiber, T., & Schmitz, A. (2000). Surrogate time series. *Physica D*, *142*, 346 – 382.

Smith, L. A. (1988). Intrinsic limits on dimension calculations. *Physics Letters A*, *133*, 283 – 288.

Theiler. J., Eubank. S., Longtin. A., Galdrikian. B., & Farmer. J. D. (1992). Testing for nonlinearity in time series: the method for surrogate data. *Physica D*, *58*, 77 – 94.

Tsuda, I. (1992). Dynamic link of memory – Chaotic memory map in nonequilibrium neural networks. *Neural Networks*, *5*, 313 – 326.

Walker, P. (1975). Stochastic properties of binocular rivalry alternations. *Perception & Psychophysics*, *18*, 467 – 473.

Wilson, H. R. (2003). Computational evidence for a rivalry hierarchy in vision. *PNAS*, *100*, 14499 – 14503.

Wilson, H. R. (2007). Minimal physiological conditions for binocular rivalry and rivalry memory. *Vision Research*, *47*, 2741 – 2750.